GAMMA-RAY BURSTS

A mega–electron volt emission line in the spectrum of a gamma-ray burst

Maria Edvige Ravasio[1,2]*, Om Sharan Salafia[2,3]*, Gor Oganesyan[4,5]*, Alessio Mei[4,5], Giancarlo Ghirlanda[2,3], Stefano Ascenzi[4,5,6,7], Biswajit Banerjee[4,5], Samanta Macera[4,5], Marica Branchesi[4,5], Peter G. Jonker[1,8], Andrew J. Levan[1,9], Daniele B. Malesani[1,10,11], Katharine B. Mulrey[1,12], Andrea Giuliani[13], Annalisa Celotti[2,14,15], Gabriele Ghisellini[2]

A long gamma–ray burst (GRB) is observed when the collapse of a massive star produces an ultrarelativistic outflow pointed toward Earth. Gamma-ray spectra of long GRBs are smooth, typically modeled by joint power-law segments describing a continuum, with no detected spectral lines. We report a significant (>6σ) narrow emission feature at ~10 mega–electron volts (MeV) in the spectrum of the bright GRB 221009A. Over 80 seconds, it evolves in energy (~12 to ~6 MeV) and in luminosity (~1.1 to <0.43 × 10^{50} erg second^{-1}) but has a constant width of ~1 MeV. We interpret this feature as a blueshifted spectral line produced by the annihilation of electron-positron pairs, potentially in the same location responsible for emitting the brightest GRB pulses.

Gamma-ray bursts (GRBs) are transient phenomena appearing as brief (from a fraction of a second up to several hundred seconds) energetic flashes of gamma rays at kilo–electron volt (keV) to mega–electron volt (MeV) energies, distributed randomly across the sky. During the intense and highly variable gamma-ray radiation phase, termed the prompt emission, an enormous amount of energy is released, typically ~10^{52} to 10^{53} erg, given the cosmological distances of GRB sources and assuming the energy is emitted isotropically. Observations and theoretical studies have shown that some GRBs are produced during the formation of stellar-mass black holes during the collapse of massive stars. The extraction of rotational energy from the black hole powers a relativistic jet; the prompt emission of GRBs is then produced by the conversion of a small fraction of the jet kinetic or magnetic energy into electromagnetic radiation (*1*, *2*).

[1]Department of Astrophysics, Institute for Mathematics, Astrophysics and Particle Physics, Radboud University, Nijmegen 6525 AJ, Netherlands. [2]Osservatorio Astronomico di Brera, Istituto Nazionale di Astrofisica, Merate 23807, Italy. [3]Sezione di Milano-Bicocca, Istituto Nazionale di Fisica Nucleare, Milan 20146, Italy. [4]Gran Sasso Science Institute, L'Aquila I-67100, Italy. [5]Laboratori Nazionali del Gran Sasso, Istituto Nazionale di Fisica Nucleare, L'Aquila I-67100, Italy. [6]Institute of Space Sciences, Consejo Superior de Investigaciones Científicas, Campus Universitat Autònoma de Barcelona, Barcelona E-08193, Spain. [7]Institut d'Estudis Espacials de Catalunya, Barcelona E-08034, Spain. [8]Netherlands Institute for Space Research, Leiden 2333 CA, Netherlands. [9]Department of Physics, University of Warwick, Coventry CV4 7AL, UK. [10]Cosmic Dawn Center, Copenhagen, Denmark. [11]Niels Bohr Institute, University of Copenhagen, Copenhagen N 2200, Denmark. [12]Nationaal Instituut voor Kernfysica en Hoge-Energiefysica, Amsterdam 1098 XG, Netherlands. [13]Istituto di Astrofisica Spaziale e Fisica Cosmica, Istituto Nazionale di Astrofisica, Milan I-20133, Italy. [14]Scuola Internazionale Superiore di Studi Avanzati, Trieste I-34136, Italy. [15]Sezione di Trieste, Istituto Nazionale di Fisica Nucleare, Trieste I-34127, Italy.
*Corresponding author. Email: mariaedvige.ravasio@ru.nl (M.E.R.); om.salafia@inaf.it (O.S.S.); gor.oganesyan@gssi.it (G.O.)

The physics of the prompt emission is poorly understood: The dominant form of energy in the relativistic jet is unknown, as is the nature of the radiative process responsible for producing the observed photons. The gamma-ray spectrum during the prompt emission phase is typically described by using a smoothly broken power-law (SBPL) model, consisting of two power laws with slopes α and β smoothly connected at a peak photon energy, E_{peak}, where most of the power is emitted. For some GRBs, detailed broad-band modeling of the spectral shape, when possible, shows fundamental deviations from that typical double power-law spectrum, such as spectral breaks at low energies (*3*, *4*) or an exponential cutoff at high energies (*5*, *6*), which can potentially provide information about the underlying physical processes.

Fermi/Gamma-Ray Burst Monitor observations of GRB 221009A

On 9 October 2022, the Gamma-Ray Burst Monitor on the Fermi spacecraft (Fermi/GBM) was triggered by GRB 221009A, an extremely bright GRB [with reported fluence $F \sim 0.2$ erg cm^{-2} (*7*–*10*)]. The redshift z of the host galaxy of GRB 221009A was measured as $z = 0.151$ (*11*). This distance and the flux at the brightest pulse of GRB 221009A result in extreme values for the isotropic equivalent gamma-ray energy $E_{iso} \sim 10^{55}$ erg and peak luminosity $L_{peak,iso} \sim 10^{54}$ erg/s (*7*–*10*). Given its extreme brightness, most gamma-ray observations of this GRB are affected by saturation effects, including those by Fermi/GBM. Analysis of Fermi/GBM data taken in time intervals affected by saturation [flagged as bad time interval (BTI)] has been discouraged (*12*).

We investigated the less bright portions of the prompt emission, outside the period flagged as BTI, over the full spectral range covered by GBM (8 keV to 40 MeV). We performed a time-resolved spectral analysis of Fermi/GBM data by extracting spectra from 0 to 460 s after the GBM trigger time and excluding the BTI from 219 to 277 s (*12*, *13*). We find that the spectra at times 280 to 320 s after the GBM trigger contain a narrow emission feature at ~10 MeV (Fig. 1). We fitted each of these spectra with a model consisting of a Gaussian representing the emission feature, superimposed on an SBPL (*13*) representing the typical GRB prompt emission continuum. Inclusion of the Gaussian component substantially improves the fitting residuals, compared with an SBPL-only model. As examples, we show the two time bins 290 to 295 s (Fig. 1, A and C) and 300 to 320 s (Fig. 1, B and D). The spectra of the other time bins are shown in fig. S9.

Figure 2A shows the light curve of GRB 221009A, as recorded by one of the sodium iodide (NaI) detectors that are part of Fermi/GBM, overlain with 13 selected time intervals (listed in table S1). We chose the time intervals on the basis of the behavior of the variable emission, ignoring times when the observed emission drops to background levels. We fitted the spectra extracted in each time interval using a range of models, including models with and without the Gaussian emission feature (*13*). Figure 2, B and C, shows the models fitted to the eight selected time intervals, spanning the first 360 s of emission (excluding the BTI). Each model is compared with the observed data in fig. S9 (*13*). Figure 2B shows the models of the four time intervals before the brightest part of the light curve; these four intervals show no evidence for the narrow emission feature. Figure 2C shows the models of the four time intervals after the BTI, which all have at least tentative evidence for the narrow feature (see "Statistical significance of the emission feature" below). The continuum component is similar in both panels [the specific functions used are described in (*13*)].

Statistical significance of the emission feature

We assess the evidence for the additional narrow emission feature using the Akaike information criterion (AIC) (*14*). Including the Gaussian component in the model improves the AIC by $\Delta AIC = 49$ and 141 in the 280 to 300 s and the 300 to 320 s time intervals, respectively, favoring its inclusion. To assess the statistical significance of the feature, we performed Monte Carlo simulations to evaluate the probability that such improvement is due to random fluctuations (*13*). Using a hypothesis-testing framework, accounting for the look-elsewhere effect [inherent in a blind search for a feature with a priori unknown properties (*15*, *16*)] and the 13 time bins analyzed, we estimated the significance as 6.2σ in the 280 to 300 s bin and 11σ in the 300 to 320 s bin. The combined significance of the feature found in multiple time bins is 13σ (*13*).

In the time intervals 7 and 8, extending from 320 to 360 s, the prompt emission has substantially faded, and modeling the spectrum requires an additional power-law component, which we attribute to the rising GRB afterglow, as seen in previous mega–electron volt observations of other bursts (*10*, *17*–*19*). Although there is tentative evidence for the Gaussian emission feature in intervals 7 and 8, at energies $7.22^{+1.63}_{-1.72}$ and $6.12^{+0.74}_{-0.59}$ MeV, respectively (Fig. 2C and fig. S9), the additional free parameters required to model the afterglow and the apparently weaker Gaussian mean that the AIC test does not favor its inclusion (ΔAIC values of −2 and 0) (Table 1) (*13*). We set 2σ upper limits on the line's luminosity of $< 0.49 \times 10^{50}$ erg s^{-1} and $< 0.43 \times 10^{50}$ erg s^{-1} in those time intervals.

If we do include the Gaussian feature in the models of intervals 7 and 8, the best-fitting parameters are well constrained (*13*) and consistent with the trend of shifting toward lower energies and lower fluxes over time (figs. S1 and S9). The peak energy of the Gaussian model component decreases over time, from an initial 12.56 ± 0.30 MeV in interval 5 to $6.12^{+0.74}_{-0.59}$ MeV in interval 8. In the 80 s between time intervals 5 and 8, the luminosity of the emission feature must have decreased by at least a factor of 2. There is no change in the best-fitting width of the emission feature. Table 1 lists the best-fitting parameters for the Gaussian emission component in our models of the time intervals 5 to 8.

Analysis of subintervals

To investigate the evolution of the emission feature at higher time resolution, we further divided intervals 5 and 6 (280 to 300 s and 300 to 320 s, respectively) into several subintervals and then repeated our modeling. Interval 5 (280 to 300 s) has the higher signal-to-noise ratio, so we subdivided it into four bins of 5 s, whereas interval 6 (300 to 320 s) was subdivided into two 10-s bins. We detect the emission feature in each of the six finer time intervals and find that it shifts from $14.40^{+0.86}_{-0.87}$ to $9.77^{+0.42}_{-0.49}$ MeV (Table 1). With the exception of subintervals 5.1 and 5.2 (Table 1), inclusion of the Gaussian component in the model is favored by the AIC test, which indicates statistical significance in the subintervals 5.3, 5.4, 6.1, and 6.2 ($\Delta AIC = 42, 5, 45$, and 36, respectively). Figure 1, A and C, shows the spectrum during subinterval 5.3. The model and the spectral data in the other subintervals are shown in fig. S10.

Comparison with other studies

The narrow feature is found in data outside the periods flagged as BTI (Fig. 2A) (*12*). An independent analysis of the same GBM spectral data in a similar time interval, from 277 to 324 s, found no evidence of instrumental problems at those times (*10*). Their analysis

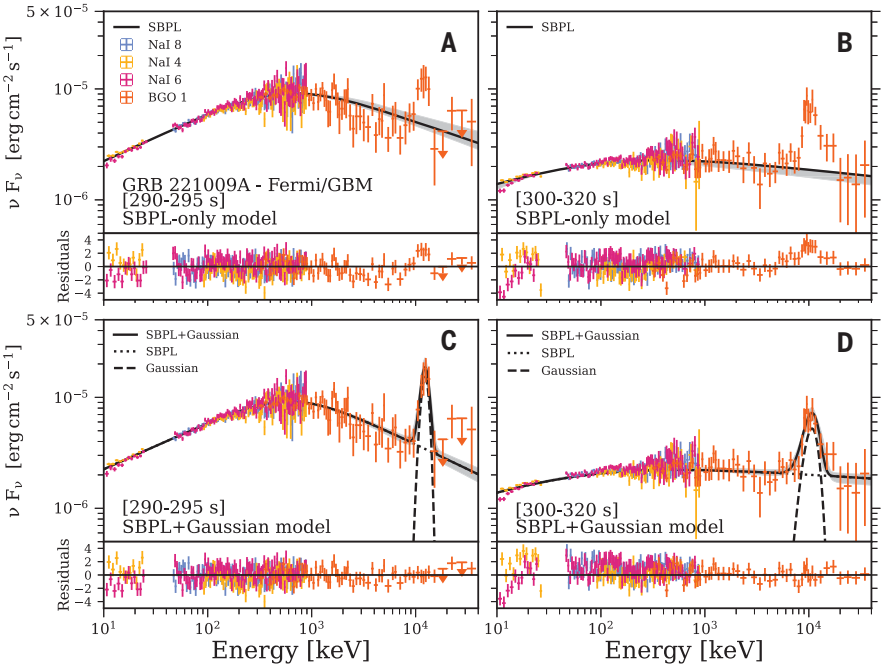

Fig. 1. GBM spectra of GRB 221009A in the time intervals 290 to 295 s and 300 to 320 s. (**A** and **B**) GBM spectra in the time intervals 290 to 295 s (interval 5.3) (A) and 300 to 320 s (interval 6) (B) overlain with an SBPL model fitted to the data. The narrow feature appears as an excess at ~10 to ~12 MeV. Data are from GBM's three sodium iodide (NaI) detectors (light blue, yellow, and purple crosses; see legend) and one BGO detector (orange crosses). Flux is shown in νF_ν representation, where ν is the photon frequency and F_ν is spectral flux as a function of frequency. (**C** and **D**) Same as (A) and (B), but with a model consisting of the SBPL (black dotted line) and an additional Gaussian emission component (black dashed lines). In all panels, data points have been rebinned at 3σ or grouped in sets of five bins for display. Error bars indicate the 1 σ uncertainty on data points, and arrows indicate upper limits at 3σ. Black lines show the best-fitting model, and gray shading represents its 1 σ uncertainty intervals. Residuals between the data and model are shown below each panel.

Table 1. Spectral parameters of the Gaussian feature. The best-fitting parameters of the Gaussian emission feature in our models are listed for time intervals 5 to 8. For intervals 5 and 6, we also list results for shorter subintervals (see text). L_{gauss} is the feature's luminosity, E_{gauss} its central photon energy, and σ_{gauss} its width. Uncertainties are 1σ, and upper limits are 2σ. ΔAIC is the change in AIC when adding the Gaussian component to the model. The corresponding best-fitting parameters for the continua in each model are listed in table S1.

Time interval (s)	Interval number	L_{gauss} (10^{50} erg s^{-1})	E_{gauss} (MeV)	σ_{gauss} (MeV)	ΔAIC
280 to 300	5	$1.12^{+0.19}_{-0.19}$	$12.56^{+0.30}_{-0.31}$	$1.31^{+0.31}_{-0.30}$	49
280 to 285	5.1	<1.5	$14.4^{+0.86}_{-0.87}$	$0.99^{+0.66}_{-0.57}$	2.4
285 to 290	5.2	<0.99	$13.2^{+6.4}_{-1.5}$	$1.14^{+0.59}_{-0.62}$	−1.2
290 to 295	5.3	$1.84^{+0.36}_{-0.33}$	$12.2^{+0.3}_{-0.3}$	$1.08^{+0.34}_{-0.30}$	42
295 to 300	5.4	$0.63^{+0.28}_{-0.27}$	$12.55^{+0.47}_{-1.4}$	$0.79^{+0.81}_{-0.45}$	5
300 to 320	6	$1.14^{+0.20}_{-0.18}$	$10.19^{+0.29}_{-0.28}$	$1.70^{+0.52}_{-0.42}$	141
300 to 310	6.1	$1.08^{+0.19}_{-0.17}$	$10.42^{+0.31}_{-0.30}$	$1.14^{+0.36}_{-0.29}$	45
310 to 320	6.2*	$0.75^{+0.21}_{-0.19}$	$9.77^{+0.42}_{-0.49}$	$1.24^{+0.25}_{-0.21}$	30
320 to 340	7*	<0.49	$7.2^{+1.6}_{-1.7}$	$2.38^{+0.45}_{-0.83}$	−2
340 to 360	8*	<0.43	$6.12^{+0.74}_{-0.59}$	$1.35^{+1.1}_{-0.74}$	0

*These spectra require an extra power-law component, representing the afterglow (see text).

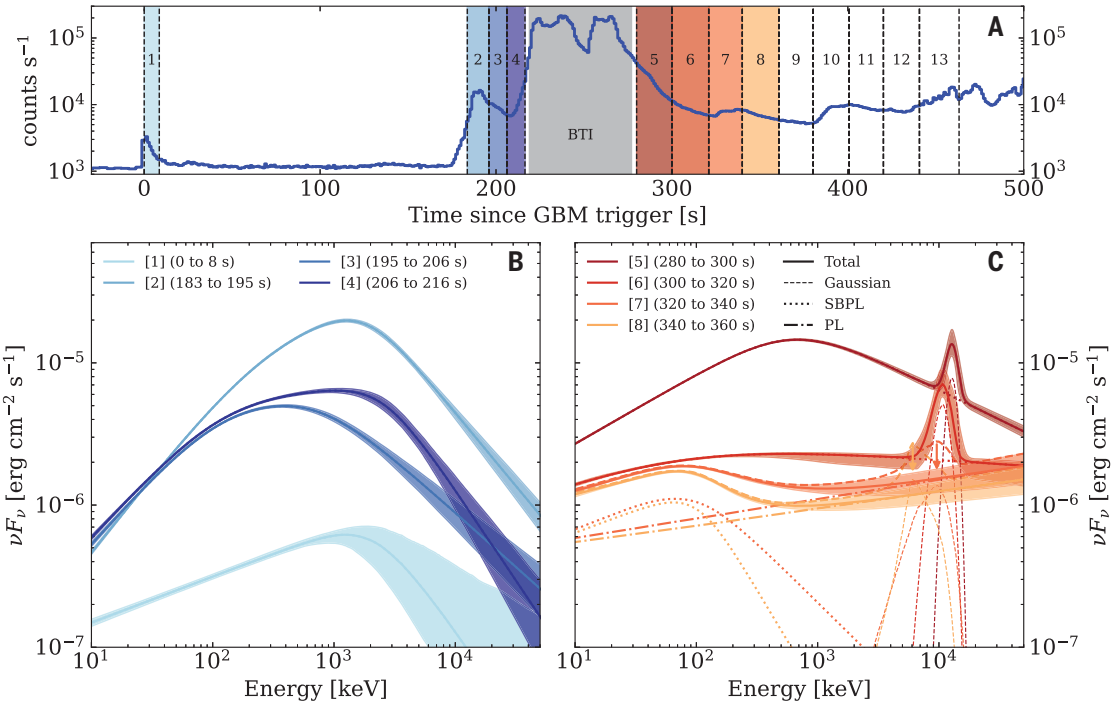

Fig. 2. GBM light curve and time-resolved spectra of GRB 221009A. (**A**) Count rate light curve of GRB 221009A (blue solid line) in the energy band 8 to 900 keV. Labeled regions are the 13 time intervals that we analyze (separated by dashed black vertical lines) and the BTI (*12*) excluded from the analysis because of detector saturation (gray shading, see text). Eight time intervals are color-coded (colors match the other panels). (**B**) Best-fitting models (solid lines) and their 90% credible intervals (shaded regions), in νF_ν representation, for time intervals 1 to 4 [colors match those in (A)]. Each model fits the data with only the typical continuum of GRB prompt emission [the specific functions used (*13*) have the parameters listed in table S1]. (**C**) Same as (B), but for time intervals 5 to 8. These models include a Gaussian emission component (dashed lines), in addition to the continuum (parameters listed in Table 1 and table S1). The continuum consists of the SBPL (dotted lines) and, for intervals 7 and 8, also a power-law model (PL) representing the afterglow (dash-dotted lines). In intervals 7 and 8, the Gaussian is not statistically significant, so its 2σ upper limits are represented with dashed lines and downward arrows. Figure S9 shows the models and data overlaid for each interval.

does show an excess of flux at 10 MeV above the fitted continuum, which they modeled using a Band function and an additional power law [figure 5 in (*10*)]. The longer integration time scale of 46 s adopted in that study (*10*) and the time evolution of the feature likely cause the excess to appear broader than the width we found in our analysis, which used 5-, 10-, and 20-s time intervals. We investigated possible instrumental origins of the emission feature (*13*) and found no evidence of an instrumental cause for the emission feature or its evolution over time. The feature also appears in the data from the other bismuth germanate (BGO) detector of GBM, with consistent spectral parameters (*13*). We searched for relevant data from other gamma-ray instruments that observed GRB 221009A but found no usable data covering the relevant time period and photon energies (*13*).

Previous studies have reported evidence for absorption or emission features in other GRBs, but none were statistically significant (>5σ). During the prompt emission phase, absorption lines at 30 to 70 keV and emission lines at 400 to 460 keV were reported for multiple bursts observed by other instruments (*20*, *21*) [one of which was interpreted as blueshifted atomic emission line (*22*)]. Another previous search for lines, mostly in absorption and < 100 keV (*23*), found no detection of any spectral line in a sample of 192 bursts (*24*). A possible transient Fe absorption feature has been reported during the prompt emission phases of GRB 990705 (*25*) and GRB 021211, with significances of 2.8σ to 3.1σ (*26*). Line searches in the afterglow emission phase revealed possible features in the soft x-ray data from four spacecraft (*27*–*33*). However, a reanalysis of those cases (*34*) argued that the statistical significances had been overestimated, so no lines were detected. An extensive search for emission or absorption lines in x-ray spectra of GRB afterglows (*35*) also did not find any statistically significant feature.

GRB 221009A differs from those cases in that we find a bright, narrow, and statistically significant emission line at several mega–electron volt energies in the Fermi/GBM spectra of a GRB. The brightness of this GRB produced a high signal-to-noise ratio in the GBM detectors, allowing the emission feature to be detected. We tested this by simulating spectra similar to those observed in interval 6 (when the feature is found with the highest significance) but with progressively lower flux, finding that a line flux 20 to 40 times lower would not have been detected above the noise (fig. S6) (*13*).

We investigated whether a similar emission feature could have been detected in other bright GRBs. We used the GBM data for the three next brightest GRBs in the energy band 10 to 1000 keV: GRB 130427A, GRB 160625B, and GRB 230307A (*13*). For each of these GRBs, we extracted the spectrum corresponding to the peak of the light curve and between two and eight spectra during the decaying phase of the pulse with the highest count rate. Although the fluxes of these spectra are 1.4 to 29 times higher than interval 6 for GRB 221009A (in the energy range of 10 keV to 40 MeV; fig. S7), none of the spectra analyzed shows evidence for an emission feature with similar width and flux. We conclude that a similar emission feature would have been detectable in those three GRBs but was not present around the time of peak brightness. We extended the search to three other GRBs, using different selection criteria [the most favorable source inclination angle with the detectors (*13*)], and found no statistically significant excess over the continuum model.

Interpretation of the emission feature

A transient, narrow emission feature at mega–electron volt energies is not predicted by standard models of GRB prompt emission (*1*, *36*–*38*). We explored several potential explanations for its presence, all assuming that the narrow spectral component is produced within the GRB

jet. The high bulk velocity of GRB jets implies a very low baryon content, so we do not expect baryons to participate in substantial nucleosynthesis. Instead, baryons remain in the form of free protons, deuterium, and (at most) α-particles (*39*). This excludes the production of observable narrow lines by fluorescent recombination within the jet. Cold electrons within the jet could conceivably interact with nearly monochromatic photons from a narrow line region that surrounds the progenitor, increasing them in energy through bulk Compton scattering (*40*, *41*), which would result in a blueshifted and Doppler-boosted emission line. We investigated this possibility but found theoretical difficulties with it (supplementary text).

Alternatively, a narrow spectral feature could arise in the form of a blueshifted electron-positron pair annihilation line. The physical conditions required to produce electron-positron pairs within the jet are probably reached in regions where energy dissipation processes (internal shocks and/or magnetic reconnection events) take place (*42*). We estimate that during the brightest pulse in GRB 221009A, a sufficient number of electron-positron pairs could have formed through two-photon annihilation within a region of the jet moving at a moderate bulk Lorentz factor $\Gamma \sim 20$ located at a radial distance $R \sim 10^{15}$ cm from the central engine (likely a black hole) (*13*). The annihilation of electron-positron pairs would then produce a spectral feature with duration, luminosity, and spectrum consistent with the one we observed. The moderate Lorentz factor $\Gamma \sim 20$ is required to place the line at ~10 MeV, as observed. This value is lower than the typical $\Gamma \gtrsim 100$ expected in powerful GRB jets and previous estimates of $\Gamma \sim 200$ to 1000 for this particular burst (*10*). Regions with lower Γ could arise temporarily (*13*) during the collision of a very fast portion of the jet with a slower one, as required for efficient energy dissipation in the leading GRB prompt emission mechanisms (*1*, *38*).

A slight modification of this scenario, which would allow for a larger Lorentz factor (possibly more in line with the expectations, given the large luminosity) and accommodate the fast evolution of the narrow feature, is for the pair annihilation line to sweep across the GBM band during the steep decline of one of the brightest pulses of the GRB, owing to the high-latitude emission effect (supplementary text) (*43*–*45*).

REFERENCES AND NOTES

1. M. J. Rees, P. Meszaros, *Astrophys. J.* **430**, L93 (1994).
2. R. Sari, R. Narayan, T. Piran, *Astrophys. J.* **473**, 204–218 (1996).
3. G. Oganesyan, L. Nava, G. Ghirlanda, A. Celotti, *Astron. Astrophys.* **616**, A138 (2018).
4. M. E. Ravasio, G. Ghirlanda, L. Nava, G. Ghisellini, *Astron. Astrophys.* **625**, A60 (2019).
5. M. Ackermann *et al*., *Astrophys. J.* **754**, 121 (2012).
6. G. Vianello *et al*., *Astrophys. J.* **864**, 163 (2018).
7. D. Frederiks *et al*., *Astrophys. J. Lett.* **949**, L7 (2023).
8. Z.-H. An *et al*., Insight-HXMT and GECAM-C observations of the brightest-of-all-time GRB 221009A. arXiv: 2303.01203 [astro-ph.HE] (2023).
9. E. Burns *et al*., *Astrophys. J. Lett.* **946**, L31 (2023).
10. S. Lesage *et al*., *Astrophys. J. Lett.* **952**, L42 (2023).
11. D. B. Malesani *et al*., The brightest GRB ever detected: GRB 221009A as a highly luminous event at z = 0.151. arXiv:2302.07891 [astro-ph.HE] (2023).
12. Fermi Collaboration, "Caveats About Analyzing GRB 221009A Data," https://fermi.gsfc.nasa.gov/ssc/data/analysis/grb221009a.html (2022).
13. Materials and methods are available as supplementary materials.
14. H. Akaike, *IEEE Trans. Automat. Contr.* **19**, 716–723 (1974).
15. K. P. Burnham, D. R. Anderson, *Sociol. Methods Res.* **33**, 261–304 (2004).
16. E. Gross, O. Vitells, *Eur. Phys. J. C* **70**, 525–530 (2010).
17. P. Meszaros, M. J. Rees, *Astrophys. J.* **405**, 278 (1993).
18. R. Sari, T. Piran, R. Narayan, *Astrophys. J.* **497**, L17–L20 (1998).
19. M. E. Ravasio *et al*., *Astron. Astrophys.* **626**, A12 (2019).
20. E. P. Mazets, S. V. Golenetskii, R. L. Aptekar, I. A. Gur'an, V. N. Ilinskii, *Nature* **290**, 378–382 (1981).
21. T. Murakami *et al*., *Nature* **335**, 234–235 (1988).
22. C. J. Hailey, F. A. Harrison, K. Mori, *Astrophys. J.* **520**, L25–L28 (1999).
23. D. L. Band *et al*., *Astrophys. J.* **458**, 746 (1996).
24. D. M. Palmer *et al*., *Astrophys. J.* **433**, L77 (1994).
25. L. Amati *et al*., *Science* **290**, 953–955 (2000).
26. F. Frontera *et al*., *Astrophys. J.* **616**, 1078–1085 (2004).
27. L. Piro *et al*., *Astron. Astrophys. Suppl. Ser.* **138**, 431–432 (1999).
28. L. A. Antonelli *et al*., *Astrophys. J.* **545**, L39–L42 (2000).
29. A. Yoshida *et al*., *Astrophys. J.* **557**, L27–L30 (2001).
30. J. N. Reeves *et al*., *Nature* **416**, 512–515 (2002).
31. D. Watson, J. N. Reeves, J. Hjorth, P. Jakobsson, K. Pedersen, *Astrophys. J.* **595**, L29–L32 (2003).
32. L. Piro *et al*., *Science* **290**, 955–958 (2000).
33. N. R. Butler *et al*., *Astrophys. J.* **597**, 1010–1016 (2003).
34. M. Sako, F. A. Harrison, R. E. Rutledge, *Astrophys. J.* **623**, 973–999 (2005).
35. S. Campana *et al*., *Astron. Astrophys.* **592**, A85 (2016).
36. G. Drenkhahn, H. C. Spruit, *Astron. Astrophys.* **391**, 1141–1153 (2002).
37. D. Lazzati, B. J. Morsony, M. C. Begelman, *Astrophys. J.* **700**, L47–L50 (2009).
38. B. Zhang, H. Yan, *Astrophys. J.* **726**, 90 (2011).
39. A. M. Beloborodov, *Astrophys. J.* **588**, 931–944 (2003).
40. M. Sikora, M. C. Begelman, M. J. Rees, *Astrophys. J.* **421**, 153 (1994).
41. M. Vietri, G. Ghisellini, D. Lazzati, F. Fiore, L. Stella, *Astrophys. J.* **550**, L43–L46 (2001).
42. A. Pe'er, E. Waxman, *Astrophys. J.* **613**, 448–459 (2004).
43. P. Kumar, A. Panaitescu, *Astrophys. J.* **541**, L51–L54 (2000).
44. G. Oganesyan *et al*., *Astrophys. J.* **893**, 88 (2020).
45. S. Ascenzi *et al*., *Astron. Astrophys.* **641**, A61 (2020).
46. O. S. Salafia, Zenodo (2024); https://doi.org/10.5281/zenodo.11635210.

ACKNOWLEDGMENTS

We thank the anonymous referees for providing constructive and valuable comments that helped improve the manuscript. We acknowledge F. C. T. Barbato for providing useful insights on the BGO detectors. This research has made use of data obtained through the High Energy Astrophysics Science Archive Research Center (HEASARC) Online Service provided by the NASA Goddard Space Flight Center. **Funding:** M.E.R. acknowledges support from the research program Athena with project number 184.034.002, which is financed by the Dutch Research Council (NWO). O.S.S. acknowledges funding by the European Union-Next Generation EU, PRIN 2022 RFF M4C21.1 (202298J7KT - PEACE). S.A. is supported by the H2020 ERC Consolidator Grant "MAGNESIA" (grant no. 817661; principal investigator: Rea) and National Spanish grant PGC2018-095512-BI00. A.J.L. and D.B.M. are supported by the European Research Council (ERC) under the European Union's Horizon 2020 research and innovation program (grant no. 725246). D.B.M. thanks the Cosmic Dawn Center, supported by the Danish National Research Foundation (grant DNRF140), for kind hospitality. G.O. and M.B. acknowledge financial support from the European Union's Horizon 2020 Programme under the AHEAD2020 project (grant no. 871158). B.B. and M.B. acknowledge financial support from the Italian Ministry of University and Research (MUR) for the PRIN grant METE under contract no. 2020KB33TP. **Author contributions:** M.E.R. extracted the Fermi data, modeled the background, performed the spectral analysis, produced figures, and led the writing of the text. O.S.S. provided the theoretical interpretations of the spectral feature, investigated the statistical significance derived from the simulations, performed the orbital background test, and contributed parts of the text. G.O. provided the theoretical interpretations of the spectral feature and contributed parts of the text. A.M. extracted and analyzed the Fermi data for the three other GRBs and contributed parts of the text. Gi.G. extracted and analyzed the Fermi data for GRB 221009A and some of the bright bursts, performed the spectral simulations and the orbital background test, and contributed parts of the text. S.A. contributed to the theoretical interpretations. B.B., S.M., M.B., P.G.J., A.J.L., D.B.M., K.B.M., and A.G. discussed the results and contributed to manuscript preparation. A.C. and Ga.G. contributed to the direction of the theoretical interpretations and manuscript preparation. **Competing interests:** The authors declare no conflicts of interest. **Data and materials availability:** The Fermi data are available from the HEASARC archive https://heasarc.gsfc.nasa.gov/db-perl/W3Browse/w3table.pl?tablehead=name%3Dfermigbrst&Action=More+Options by searching for "GRB221009553" in the "name" field. The results of our model fitting are listed in Table 1 and table S1. Our code to derive the background using the orbital method is available at https://github.com/omsharansalafia/GBM_bkg_orbital_method and archived at Zenodo (*46*).

SUPPLEMENTARY MATERIALS

science.org/doi/10.1126/science.adj3638
Materials and Methods
Supplementary Text
Figs. S1 to S11
Table S1
References (*47*–*81*)

Submitted 23 June 2023; accepted 14 June 2024
10.1126/science.adj3638